Available online at www.sciencedirect.com
SCIENCE DIRECT
Chemico-Biological Interactions 157–158 (2005) 153–157
Chemico-Biological Interactions
www.elsevier.com/locate/chembioint

The 3D structure of the anticancer prodrug CPT-11 with *Torpedo californica* acetylcholinesterase rationalizes its inhibitory action on AChE and its hydrolysis by butyrylcholinesterase and carboxylesterase

Michal Harel [a,*], Janice L. Hyatt [b], Boris Brumshtein [a], Christopher L. Morton [b], Randy M. Wadkins [c], Israel Silman [d], Joel L. Sussman [a], Philip M. Potter [b]

[a] *Department of Structural Biology, Weizmann Institute of Science, Rehovot 76100, Israel*
[b] *Department of Molecular Pharmacology, St. Jude Children's Research Hospital, 332 N. Lauderdale, Memphis, TN 38105, USA*
[c] *Department of Chemistry and Biochemistry, University of Mississippi, University, MS 38677, USA*
[d] *Department of Neurobiology, Weizmann Institute of Science, Rehovot 76100 Israel*

Available online 14 November 2005

Abstract

The anticancer prodrug CPT-11 is a highly effective camptothecin analog that has been approved for the treatment of colon cancer. The 2.6 Å resolution crystal structure of its complex with *Torpedo californica* acetylcholinesterase (*Tc*AChE) demonstrates that CPT-11 binds to *Tc*AChE and spans its gorge similarly to the Alzheimer drug, Aricept. The crystal structure clearly reveals the interactions, which contribute to the inhibitory action of CPT-11. Modeling of the complexes of CPT-11 with mammalian butyrylcholinesterase and carboxylesterase, both of which are known to hydrolyze the drug, shows how binding to either of the two enzymes yields a productive substrate-enzyme complex.

Keywords: Anticancer prodrug; Cholinergic syndrome; X-ray crystallography; Alzheimer; Colon cancer

1. Introduction

CPT-11 (Camptosar, irinotecan, 7-ethyl-10-[4-(1-piperidino)-1-piperidino]carbonyloxycamptothecin) is a camptothecin-derived prodrug that is activated by carboxylesterases (CEs) to yield the potent topoisomerase poison SN-38 (7-ethyl-10-hydroxycamptothecin) [1]. CPT-11 has demonstrated good antitumor activity against both drug-naïve and resistant tumors, and is approved for the treatment of colon cancer. It is currently being assessed for efficacy towards a variety of solid tumors both in adults and children [2–5].

CPT-11 is a carbamate that requires cleavage by CEs to yield SN-38 as shown:

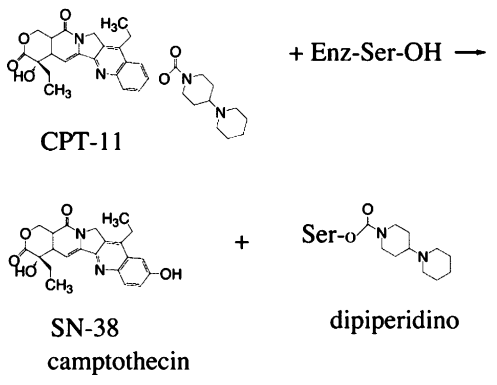

* Corresponding author.

0009-2797/$ – see front matter © 2005 Elsevier Ireland Ltd. All rights reserved.
doi:10.1016/j.cbi.2005.10.016

During i.v. administration of CPT-11, a cholinergic syndrome is frequently observed [6–9]. These symptoms can be rapidly alleviated by atropine, suggesting that the side effects result from interaction of the parent drug with acetylcholinesterase (AChE).

We, and others, have demonstrated that CPT-11 can directly inhibit both human and eel AChE [10–12], whereas it can be activated by butyrylcholinesterase (BChE). To understand the mechanism of inhibition of AChE by CPT-11, we have undertaken to solve the X-ray structure of this complex.

2. Results

2.1. 3D structure of the CPT-11/TcAChE complex

The 3D-structure of the complex of *Tc*AChE and CPT-11 at 2.6 Å resolution was solved from X-ray data collected from a single crystal of *Tc*AChE grown in the presence of gallamine triethiodide (Brumshtein, personal communication), and soaked in a solution containing CPT-11. The crystals belong to space group $P3_221$. In this crystal form, the entrance to the active-site gorge is not blocked by a symmetry-related molecule as is the case for the $P3_121$ trigonal *Tc*AChE crystals (PDB code 1EA5). The RMS deviation of the Cα chain between the $P3_221$ and the $P3_121$ crystals is only 0.3 Å, indicating an identical conformation of the two *Tc*AChE 3D structures. The final complex structure refined to an *R*-factor of 18.7% and *R*-free of 23.7%. The electron density of this complex allowed tracing of residues 4-536 of *Tc*AChE, and showed the location of CPT-11, 241 water molecules, and 3 out of 4 putative *Tc*AChE glycosylation sites. An iodide ion interacting with the side-chains of His264 and Glu268 was also observed, which displayed 60% occupancy. The electron density shows glycosidic bonding of Asn59-*N*-acetylglucosamine (NAG)-fucose (FUC); Asn416-NAG-NAG, and a branched Asn457-NAG(FUC)-NAG-mannose.

The CPT-11 molecule spans the active-site gorge, interacting with a series of residues from Trp84 at the bottom of the gorge to Phe284 in the topmost loop (Fig. 1). Nine of the 13 amino acids with which CPT-11interacts are aromatic (Tyr70, Trp84, Tyr121, Trp279, Phe284, Phe330, Phe331, Tyr334, His440), and the drug thus makes numerous contacts with the protein.

2.2. Overlay of the CPT-11/TcAChE complex with the hBChE and rabbit liver CE structures

We earlier reported that whilst CPT-11 is a potent inhibitor of AChE, both hBChE and CEs can activate the drug to yield SN-38 [10]. Predictive computer modeling, based upon the *Tc*AChE crystal structure, indicated that the active site of hBChE was large enough to accommodate the drug, and that the carbamate function can be positioned so as to allow nucleophilic attack by the active-site serine, Ser198 [10]. To confirm this prediction, we overlaid the CPT-11/*Tc*AChE complex structure on that of hBChE (PDB code 1P0I), with a Cα RMS deviation of 0.8 Å for 448 amino acid residues. Modeling the drug in the active-site gorge with the carbamate carbonyl oxygen within bonding distance of Ser198 Cβ, resulted in a CPT-11/hBChE model of exquisite fit (Fig. 2). In

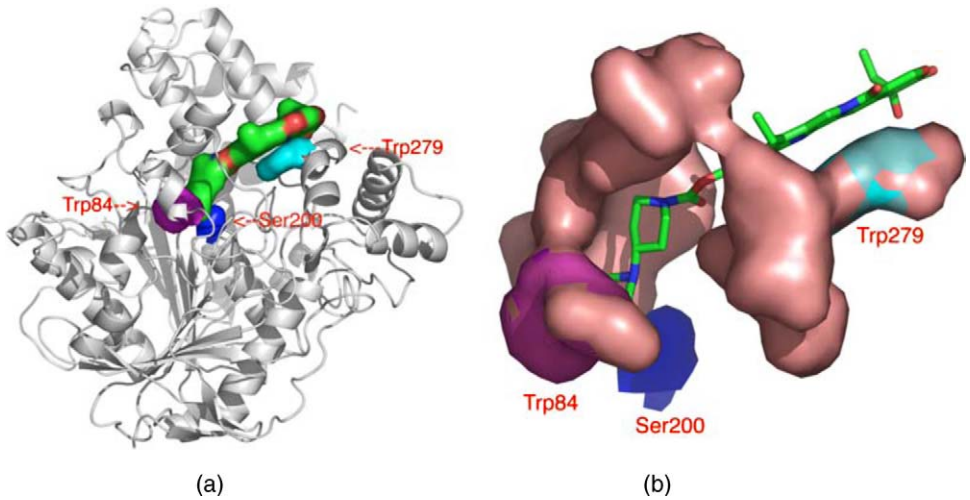

Fig. 1. Crystal structure of the CPT-11/*Tc*AChE complex. (a) CPT-11 is shown in green as a space-filling structure spanning the active-site gorge. Trp279 is shown in cyan, Trp84 in magenta, and Ser200, which is too far from the hydrolysable CPT-11 ester bond to interact with it, is shown in blue. (b) Stick model of CPT-11 with all *Tc*AChE residues that are at a distance <3.0 Å from it. Figure made using PyMOL [13].

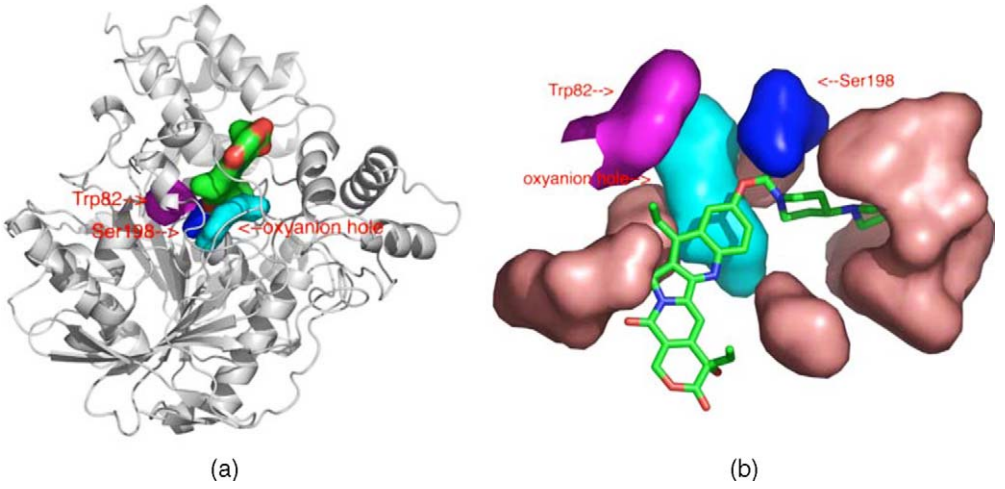

Fig. 2. Model structure of the complex of CPT-11 with hBChE. (a) CPT-11 is shown in green as a space-filling structure spanning the active-site gorge. Ser198, whose Oγ atom is within bonding distance of the carbonyl carbon of CPT-11, is shown in blue, the oxyanion hole residues are shown in cyan, and Trp82 is shown in magenta. (b) Stick model of CPT-11 together with all hBChE residues at a distance <3.0 Å from it. Figure made using PyMOL [13].

this model, Trp231 χ1 is rotated by 110° away from its native conformation in hBChE to avoid steric clashes between CPT-11 and the rest of the protein. The CPT-11/hBChE model was subjected to 90 cycles of energy minimization using program CNS [14] to minimize van der Waals clashes between CPT-11 and hBChE. This minimization resulted in the total energy dropping from 6290 to 2819 kcal, and the van der Waals energy from 1575 to 922 kcal.

The X-ray structure of a rabbit liver CE (rCE; PDB code 1K4Y [15]) was similarly fitted to the CPT-11/*Tc*AChE structure, and displayed a Cα RMS deviation of 0.9 Å for 285 residues (Fig. 3). Here again, CPT-11 was positioned so that the carbamate carbonyl oxygen was within bonding distance of Ser221 Cβ, and the dipiperidino and camptothecin moieties were subjected to torsion angle rotation to avoid steric clashes with the rCE structure. The CPT-11/rCE model was subjected to 90 cycles of energy minimization and the total energy dropped from 4846 to 2256 kcal, and the van der Waals energy from 1536 to 794 kcal.

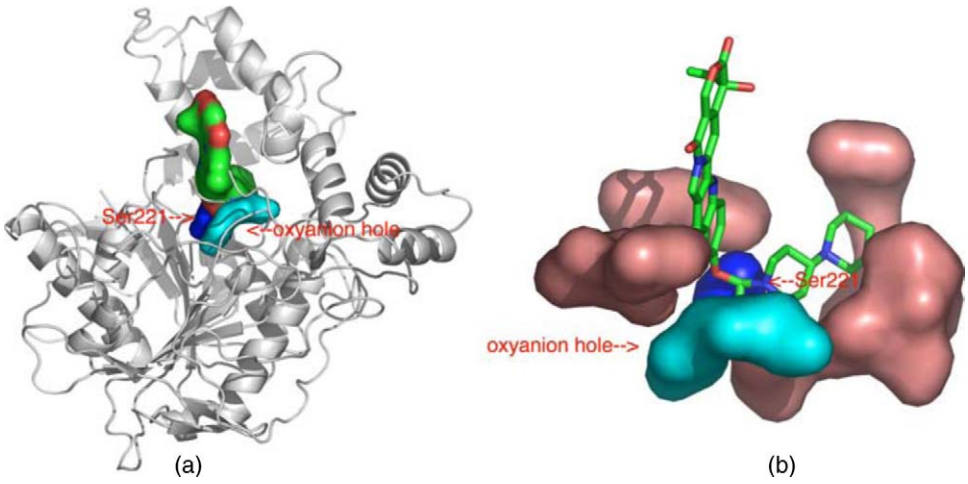

Fig. 3. Model structure of the complex of CPT-11 with rCE. (a) CPT-11 is shown in green as a space-filling structure spanning the active-site gorge. Ser221, whose Oγ atom is within bonding distance of the carbonyl carbon of CPT-11, is shown in blue, the oxyanion hole residues are shown in cyan. (b) Stick figure model of CPT-11 together with all rCE residues at a distance <3.0 Å from it. Figure made using PyMOL [13].

3. Discussion

The crystal structure of its complex with *Tc*AChE revealed that CPT-11 aligns within the active-site gorge of the enzyme very similarly to Aricept (PDB code 1EVE). Stabilization of the drug within the active-site gorge is achieved by numerous π–π stacking interactions of the camptothecin rings with those of the aromatic amino acids that line the catalytic gorge. In particular, interactions of the fused aromatic rings with the indole group of Trp279, which is part of the peripheral binding site of the enzyme, demonstrates remarkable similarity to the stacking of the indanone moiety of Aricept. Thus, the potency of CPT-11 as an AChE inhibitor is due to several factors: firstly, the dipiperidino rings occupy the anionic subsite of the active site, and the ultimate piperidino ring, is tilted by ca. 30° relative to the plane of the indole ring of Trp84. Secondly, the camptothecin ring system (consisting of 4 aromatic rings and a cyclic lactone) allows for extensive interactions with the numerous tyrosine, tryptophan and phenylalanine residues that line the upper part of the active-site gorge. Finally, the dimensions of CPT-11 and the catalytic gorge are such that the drug fits very 'snugly' along the entire length of the gorge. This combination of factors results in effective AChE inhibition by CPT-11.

While CPT-11 inhibits AChE, we, and others, have demonstrated that BChE can hydrolyze the drug to SN-38 [10,11]. This implies that the carbamate moiety of CPT-11, located between the dipiperidino moiety and the fused aromatic rings, should be within bonding distance of the active-site serine Cβ. The overlay of the CPT-11/*Tc*AChE structure with that of hBChE (PDB code 1P0I) shows that the loop present at the top of the active-site gorge (residues 282-286 in *Tc*AChE) has a different conformation in the two closely related enzymes. This loop makes numerous interactions with CPT-11 in *Tc*AChE, but its position in hBChE does not allow the drug to occupy the upper part of the gorge. Moving the drug down the gorge to avoid clashes with the corresponding loop in hBChE (residues 280-284), brings the carbamate moiety within bonding distance of Ser198 Cβ, resulting in a model of the CPT-11/*h*BChE complex in which the CPT-11 fits very snugly. BChE lacks the key AChE peripheral binding site residue Trp279, which is replaced by Ala277. This difference results in failure of CPT-11 to inhibit BChE [16], since its camptothecin moiety does not make strong π–π stacking interactions at the top of the gorge.

Recently, we determined the X-ray structure of *r*CE that can efficiently activate CPT-11 [15]. Comparison of its structure with that of *Tc*AChE revealed that their folds are very similar, with a Cα RMS deviation of 0.9 Å for 285 amino acid residues. While they have very different substrate specificities, it is clear that their structures are evolutionarily conserved. The rCE structure in the area corresponding to that of the *Tc*AChE peripheral binding site is very different from that of the latter, with Lys301 occupying the position of *Tc*AChE Trp279. In addition, in rCE, as in hBChE, there are no aromatic side chains at the top of the active-site gorge, which could make π–π stacking interactions of sufficient strength to prevent CPT-11 accessing the amino acids of the catalytic triad. In particular, Trp279 in the CPT-11/*Tc*AChE structure makes 8 π–π stacking interactions with rings B and C of the camptothecin moiety. Hence, the CPT-11/*Tc*AChE structure differs markedly from the models obtained using the hBChE and rCE X-ray structures, explaining the inhibition of the former by CPT-11, rather than the hydrolysis observed with the latter two enzymes.

Overall, the data presented here demonstrates that CPT-11 is a potent inhibitor of AChE, and that this is primarily mediated by the piperidino rings binding within the anionic subsite of the protein. In addition, the complex is stabilized by aromatic π–π stacking interactions between the camptothecin rings and aromatic amino acids that line the active-site gorge, and in particular with Trp279 within the *Tc*AChE peripheral binding site.

4. Methods

*Tc*AChE crystals were grown by the vapor diffusion method, using a 1.5 μl drop of a solution of 10 mg/ml protein mixed with 1.5 μl of mother liquor at 4 °C. The mother liquor solution contained 25% PEG 600 in 0.05 M HEPES, pH 7.5, and 0.027 M gallamine triethiodide, which was added in order to produce crystals of spacegroup $P3_221$ (Brumshtein, unpublished results). Trigonal crystals with dimensions of 0.2 mm × 0.1 mm grew within 3 weeks. The complex with CPT-11 was obtained by transferring the crystals to a saturated solution of CPT-11 in mother liquor for 16 h. X-ray data were collected from a single crystal, on an *R*-axis diffractometer at 100 K, after washing the mother liquor off the crystal with Parathone N oil. The data were processed using XDS [17], and the structure was solved by molecular replacement, using the $P3_221$ native *Tc*AChE structure as a starting model. Data were refined using CNS [14] and fitted using O [18]. Data processing and refinement statistics are shown below:

Data collection	
Wavelength (Å)	1.54
Unit cell (Å)	137.75, 70.87
Space group	$P3_221$
Resolution range (Å)	30-2.6
Number of unique reflections	23,798
Completeness (%)[a]	98.5 (90.9)
$I/\sigma(I)$[a]	10.3 (4.7)
$R_{sym}(I)$ (%)[a]	8.0 (24.0)
Refinement and model statistics	
Resolution range (Å)	30–2.6
Number of reflections	23,820
R-factor: work, free (%)	18.7, 23.7
Average B-factors (Å^2)	39.9
RMSD from ideal values	
Bond length (Å)	0.007
Bond angle (°)	1.3
Dihedral angles (°)	21.7
Improper torsion angles (°)	0.88
Estimated coordinate error	
Low resolution cut-off (Å)	5.0
ESD from Luzzati plot (Å)	0.28
ESD from SIGMAA (Å)	0.42
Ramachandran outliers (%)	3.3

[a] Data for the outer shell are given in parentheses.

Acknowledgements

This work was supported in part by an NIH Cancer Center Core Grant P30-CA-21765, and the American Lebanese Syrian Associated Charities.

References

[1] A. Tanizawa, A. Fujimori, Y. Fujimori, Y. Pommier, Comparison of topoisomerase I inhibition, DNA damage, and cytotoxicity of camptothecin derivatives presently in clinical trials, J. Natl. Cancer Inst. 86 (1994) 836–842.
[2] W.L. Furman, et al., Direct translation of a protracted irinotecan schedule from a xenograft model to a Phase I trial in children, J. Clin. Oncol. 17 (1999) 1815–1824.
[3] N. Saijo, Progress in treatment of small-cell lung cancer: role of CPT-11, Br. J. Cancer 89 (2003) 2178–2183.
[4] C.J. Langer, The global role of irinotecan in the treatment of lung cancer: 2003 update, Oncology 17 (2003) 30–40.
[5] M. Simon, A. Argiris, J.R. Murren, Progress in the therapy of small cell lung cancer, Crit. Rev. Oncol. Hematol. 49 (2004) 119–133.
[6] D. Gandia, et al., CPT-11-induced cholinergic effects in cancer patients [letter], J. Clin. Oncol. 11 (1993) 196–197.
[7] D. Abigerges, et al., Phase I and pharmacologic studies of the camptothecin analog irinotecan administered every 3 weeks in cancer patients, J. Clin. Oncol. 13 (1995) 210–221.
[8] R. Bugat, et al., Efficacy of irinotecan HCl (CPT11) in patients with metastatic colorectal cancer after progression while receiving a 5-FU-based chemotherapy, Proc. Annu. Meet. Am. Soc. Clin. Oncol. 14 (1995) A567 (meeting abstract).
[9] R.G. Petit, M.L. Rothenberg, E.P. Mitchell, L.D. Compton, L.L. Miller, Cholinergic symptoms following CPT-11 infusion in a phase II multicenter trial of 250 mg/m^2 irinotecan (CRT-11) given every two weeks, Proc. Annu. Meet. Am. Soc. Clin. Oncol. 16 (1997) A953 (meeting abstract).
[10] C.L. Morton, R.M. Wadkins, M.K. Danks, P.M. Potter, CPT-11 is a potent inhibitor of acetylcholinesterase but is rapidly catalyzed to SN-38 by butyrylcholinesterase, Cancer Res. 59 (1999) 1458–1463.
[11] H.M. Dodds, L.P. Rivory, The mechanism for the inhibition of acetylcholinesterases by irinotecan (CPT-11), Mol. Pharmacol. 56 (1999) 1346–1353.
[12] Y. Kawato, et al., Inhibitory activity of camptothecin derivatives against acetylcholinesterase in dogs and their binding activity to acetylcholine receptors in rats, J. Pharm. Pharmacol. 45 (1993) 444–448.
[13] W.L. DeLano, PyMOL is a user-sponsored molecular modeling system, http://pymol.sourceforge.net.
[14] A.T. Brunger, et al., Crystallography & NMR system: a new software suite for macromolecular structure determination, Acta Cryst. 54 (Pt 5) (1998) 905–921.
[15] S. Bencharit, et al., Structural insights into CPT-11 activation by mammalian carboxylesterases, Nat. Struct. Biol. 9 (2002) 337–342.
[16] Z. Radic, E. Reiner, P. Taylor, Role of the peripheral anionic site on acetylcholinesterase: inhibition by substrates and coumarin derivatives, Mol. Pharmacol. 39 (1991) 98–104.
[17] W. Kabsch, Automatic processing of rotation diffraction data from crystals of initially unknown symmetry and cell constants, J. Appl. Cryst. 26 (1993) 795–800.
[18] T.A. Jones, J.Y. Zou, S.W. Cowan, Kjeldgaard, Improved methods for building protein models in electron density maps and the location of errors in these models, Acta Cryst. 47 (Pt 2) (1991) 110–119.